Eurasian Journal of Physics and Functional Materials

Volume 9 | Number 3

Article 4

Pages: 1 - 1

2025

Zinc Oxide Nanoparticles Synthesized from Zinc(II)-2-Acetylpyrazine-4-Methylthiosemicarbazone Complex and Coffea Liberica Extract: Catalysis Study

Anis Syahirani Mohd Zaini
Chemical Sciences, Faculty of Science, University Brunei Darussalam, Jalan Tungku Link, Gadong BE 1410, Brunei Darussalam

Ai Ling Tan
Chemical Sciences, Faculty of Science, University Brunei Darussalam, Jalan Tungku Link, Gadong BE 1410, Brunei Darussalam

Wan Nor Roslam Wan Isahak
Department of Chemical and Process Engineering, Faculty of Engineering and Built Environment, Universiti Kebangsaan Malaysia, 43600 UKM, Selangor, Malaysia

Malai Haniti Sheikh Abdul Hamid
Chemical Sciences, Faculty of Science, University Brunei Darussalam, Jalan Tungku Link, Gadong BE 1410, Brunei Darussalam, haniti.hamid@ubd.edu.bn

Recommended Citation

Mohd Zaini, Anis Syahirani; Tan, Ai Ling; Wan Isahak, Wan Nor Roslam; and Sheikh Abdul Hamid, Malai Haniti (2025) "Zinc Oxide Nanoparticles Synthesized from Zinc(II)-2-Acetylpyrazine-4-Methylthiosemicarbazone Complex and Coffea Liberica Extract: Catalysis Study," *Eurasian Journal of Physics and Functional Materials*: Vol. 9: No. 3, Article 4.
DOI: https://doi.org/10.69912/2616-8537.1253

ORIGINAL STUDY

Zinc Oxide Nanoparticles Synthesized From Zinc(II)-2-acetylpyrazine-4-methylthiosemicarbazone Complex and *Coffea liberica* Leaf Extract: Catalysis Study

Anis S. Mohd Zaini [a], Ai Ling Tan [a], Wan N.R. Wan Isahak [b], Malai Haniti S.A. Hamid [a,*]

[a] Chemical Sciences, Faculty of Science, University Brunei Darussalam, Jalan Tungku Link, Gadong BE 1410, Brunei Darussalam
[b] Department of Chemical and Process Engineering, Faculty of Engineering and Built Environment, Universiti Kebangsaan Malaysia, 43600 UKM, Selangor, Malaysia

Abstract

The increasing demand for sustainable catalysts is a significant challenge in the industrial sector. Traditional catalytic processes often rely on harmful chemicals and high-energy inputs, contributing to environmental pollution. In this work, we investigate the catalytic activity of chemically synthesized zinc oxide nanoparticles (ZnO NPs) derived from zinc(II) 2-acetylpyrazine-4-methylthiosemicarbazone as a precursor (ZnO-SB), and green synthesized ZnO NPs derived from three different concentrations of leaf extracts of *Coffea liberica* leaf extract (ZnO-1, ZnO-5, and ZnO-10). ZnO-5 has been shown to exhibit a rodlike structure and highly porous morphology, while ZnO-1, ZnO-10, and ZnO-SB exhibit irregular and spherical structures with less porous morphology. FTIR spectra shows that the medium intense bands of Zn-O stretching were observed at approximately 400 cm^{-1} for ZnO-SB, ZnO-1, ZnO-10, and ZnO-C, while 409 cm^{-1} for ZnO-5. All the synthesized ZnO NPs were investigated as a catalyst in the acylation of phenol and it was shown that the green synthesized ZnO NPs are more favorable, specifically ZnO-5. A reusability test for ZnO-5 observed that this catalyst can be reused many times without significant loss in its activity. X-ray diffraction of ZnO NP shows that it crystallizes in hexagonal wurtzite phase and the average particle sizes of ZnO-1, ZnO-5, ZnO-10, and ZnO-SB were 42.18 nm, 40.56 nm, 34.34 nm, and 51.80 nm, respectively. This study shows that green synthesized ZnO NPs are potential catalysts in organic reactions. The results also show that the green synthesized ZnO NPs are more porous than chemically synthesized ZnO NPs. The synthesized ligand (L) and its zinc(II) complex (ZnL_2) were characterized by FTIR, UV-Vis, and MS spectroscopic techniques.

Keywords: Thiosemicarbazone, Zn(II) Schiff base complex, ZnO NPs, Aqueous *Coffea liberica* leaf extract, Catalytic reaction

1. Introduction

Catalysts have been fundamental to advancement in modern chemistry and served as a foundation for the transformation of industrial development. Starting from early civilizations using fire to accelerate reactions, the quest for catalytic processes has continued through history, evolving into today's applications that drive innovation across numerous industries. Catalysts operate based on their ability to have an alternative pathway that lowers the activation energy, thus facilitating a faster and more efficient process. By reducing the activation energy barrier, catalysts can make reactions economically and technologically viable, which is key to chemical manufacturing [1,2]. Advances in catalyst technology, such as novel catalysts for alcohol oxidation with pharmaceutical applications and those for organic oxidation in environmental remediation, underscore their importance [3,4]. Catalysts are categorized as homogeneous or heterogeneous catalysts.

Received 21 May 2025; revised 28 June 2025; accepted 29 July 2025.
Available online 7 October 2025

* Corresponding author.
E-mail address: haniti.hamid@ubd.edu.bn (M.H.S.A. Hamid).

https://doi.org/10.69912/2616-8537.1253

While homogeneous catalysts are known to provide better selectivity, heterogeneous catalysts are preferred for ease of recovery and reusability. Among heterogeneous catalysts, metal oxide nanoparticles, including zinc oxide nanoparticles (ZnO NPs), have garnered significant attention for their high surface area-to-volume ratio and distinctive electronic properties, excelling in reactions, e.g., dehydrogenation, Claisen-Schmidt, transesterification, and acylation [5−10]. These nanocatalysts offer superior reactivity, selectivity, and reusability, driving sustainable organic synthesis. Acylation reaction protects hydroxyl groups during synthesis and finds applications in industries such as pharmaceuticals and cosmetics [8]. Traditionally catalyzed by acids or bases, modern alternatives, including ZnO NPs, provide milder conditions and higher yields [11,12]. The nanotechnology revolution has enhanced the performance of ZnO NPs which exhibit unique properties due to their nanoscale dimensions. ZnO NPs, known for their biocompatibility and low toxicity, are utilized in applications ranging from antibacterial agents to drug delivery systems [13]. Among the synthesis approaches, chemical methods such as thermal decomposition offer precise control over particle size and purity. For instance, using hydrazone Schiff base (SB) shows the use of ZnO NPs as a catalyst for Biglini reactions, which shows faster, higher yield, and easy recovery of the catalyst [14]. Green synthesis using plant extracts provides environmentally friendly alternatives [15,16]. With these two methods, thiosemicarbazone (TSC) enhances ZnO NPs synthesis, particularly through coordination chemistry with metal ions. A notable TSC ligand is 2-acetylpyrazine-4-methylthiosemicarbazone, specifically, the bulky group at the N^4 position of the TSC scaffold can further enhance the biological efficacy of these compounds, making them promising candidates for therapeutic applications [17−19].

The *Coffea* genus, scientifically known as the *Rubiaceae family*, is a globally popular beverage valued for its pleasant flavor, stimulating effect, and possible health advantages such as reduced risks of type 2 diabetes and colorectal cancer [20,21]. While *Coffea arabica* and *Coffea robusta* dominate cultivation, *Coffea liberica* characterized by its tall growth, hardy nature, and large leaves remains understudied [22]. The phytochemicals of *Coffea liberica* leaf extract has revealed a diverse array of bioactive compounds e.g. alkaloids, flavonoids, and saponins, which contribute to its antioxidant and potential therapeutic applications [23]. These diverse phytochemicals also facilitated the synthesis of ZnO NPs by acting as reducing and stabilizing agents during nanoparticle formation [24−26]. Thus, in the present study, ZnO NPs were synthesized by chemical method via thermal decomposition of zinc(II) complex from 2-acetylpyrazine-4-methylthiosemicarbazone (ZnL_2) as a precursor and green synthesis using *Coffea liberica* leaf extract, where the phytochemicals present in the leaf extract act as capping and stabilizing agents. Detailed investigation of the particle size and morphology of the synthesized ZnO NPs was also discussed. For the first time, this paper reports the influence of ZnO NPs from both chemical and green methods on the catalytic organic reaction of acylation of phenol.

2. Experimental

2.1. Materials and instrumentation

Coffea liberica leaves were collected from Labi Coffee Farm, Belait District, Brunei Darussalam. Zinc(II) nitrate hexahydrate, ($Zn(NO_3)_2 \cdot 6H_2O$, 98 %), 2-acetylpyrazine (97 %) and 4-methyl-3-thiosemicarbazide (97 %) were all purchased from Sigma-Aldrich. Methanol (≥99.5 %), acetonitrile, dichloromethane, phenol, 2-naphthol, and anhydrous sodium sulfate were all obtained from Merck. In addition, sodium bicarbonate, petroleum ether 40−60 °C, 4-chlorophenol, and ethyl acetate were all from BDH, while benzoyl chloride and zinc(II) acetate dihydrate ($Zn(CH_3CO_2)_2 \cdot 2H_2O$, 98 %) were obtained from Fluka. For comparison purposes, commercial ZnO (ZnO-C) was used. Absolute ethanol was purchased from Scharlay, while the other chemical reagents, including glacial acetic acid, were obtained from Univar. All the chemical reagents were used without further purification. Attenuated Total Reflectance-Fourier Transform Infrared (ATR-FTIR) spectra were obtained from a Shimadzu IR Prestige-21, Fourier Transform Infrared Spectrometer. PANalytical AERIS X-ray diffractometer was used to get X-ray diffraction (XRD) using Cu Kα radiation (0.15406 nm) in the range of 2θ from 20° to 80°. Thermolyne 1400 furnace for calcination of ZnO NPs, Shimadzu UV-1900 UV-Vis spectrometer using DMSO as a solvent was used, and the spectra were plotted using Origin Lab. ImageJ and Chemsketch software were used to calculate the average particle size of synthesized ZnO NPs and for chemical structures, respectively. The FESEM-EDX and CHN were carried out at the i-CRIM Centralised Lab, Universiti Kebangsaan Malaysia. Mass spectra were recorded on an Agilent 6546 LC-QTOF at the National University of Singapore (NUS).

2.2. Chemical synthesis of ZnO from zinc(II) schiff base complex

2.2.1. Preparation of ligand, 2-acetylpyrazine 4-methylthiosemicarbazone [L]

The preparation of L was adapted from Zhou et al. [19], where a solution of 2-acetylpyrazine (0.2444 g, 2

mmol) in absolute ethanol was mixed with a solution of 4-methyl-3-thiosemicarbazide (0.2104 g, 2 mmol) in absolute ethanol with 4 drops of glacial acetic acid added. The solution mixture was refluxed for 30 minutes, pale-yellow crystals product formed, which were filtered off, washed with cold absolute ethanol, and recrystallized from acetonitrile and methanol to obtain pale-yellow crystals. Yield: 0.1874 g, 45 %; m.pt: 242−244 °C. Elemental analysis for $C_8H_{11}N_5S$ calcd (%): C, 47.98; H, 5.64; N, 33.57. Found: C, 51.60; H, 5.69; N, 36.34. FTIR (υ_{max}, cm^{-1}): 3303, 3214 *ν*(N−H), 1543 *ν*(C=C arom), 1607 *ν*(C=N), 840 *ν*(C=S). UV-Vis (DMSO), λ_{max} nm: 250, 328. HR-ESI-MS calculated for $C_8H_{11}N_5S$ $[M+H]^+$: 209.28, Found: 210.10.

2.2.2. Synthesis of Zinc(II) complex [ZnL_2]

Zinc(II) acetate dihydrate (0.0262 g, 0.120 mmol) was dissolved and heated in a solution of methanol (5 mL). By using a 1:2 metal-ligand ratio, the mixture was added to the ligand solution, L (50 mg, 0.239 mmol) dissolved in acetonitrile and methanol to form an orange solution. The mixture was then refluxed for 6 hours and left to stand overnight to yield an orange powder. The product was filtered, washed with cold acetonitrile, and air-dried. Yield: 0.0289 g, 30 %, m.pt: 262 °C (decomposed). Elemental analysis for $ZnC_{16}H_{20}N_{10}S_2$ calcd (%): C, 39.88; H, 4.18; N, 29.06. Found: C, 40.33; H, 4.15; N, 26.54. FTIR (υ_{max}, cm^{-1}): 3260 *ν*(N−H), 1543 *ν*(C=C arom), 1577 *ν*(C=N), 821 *ν*(C=S). UV-Vis (DMSO), λ_{max} nm: 248, 322, 421. HR-ESI-MS calculated for $ZnC_{16}H_{20}N_{10}S_2$ $[M+H]^+$: 481.92, Found: 481.10.

2.2.3. Synthesis of ZnO NPs [ZnO-SB]

The ZnO-SB was prepared by thermal decomposition of ZnL_2 (1 g) at 600 °C for 2 h. Afterward, the crucibles were placed in the muffle furnace and calcined to produce a cream fine powder. Fig. 1 illustrates the summary of the synthesis of ZnO NPs derived from the Zn(II) Schiff base complex.

2.3. Green synthesis of ZnO NPs

2.3.1. Preparation of aqueous Coffea liberica *leaf extract*

The leaves were collected and washed thrice with tap water, followed by distilled water to remove the dust particles. The leaves were then air-dried and dehydrated for 7 hours using a Dessini, DS-350A dehydrator until constant weighed. The dehydrated leaves were then cut and blended into a fine powder. The desired weighed powder (1 g, 5 g, or 10 g) was transferred to a 100 ml conical flask with 50 mL of distilled water and sonicated for 1 h at 60 °C. After sonication, the conical flask was cooled at room temperature and vacuum filtered to collect the aqueous leaf extract for 1 g, 5 g and 10 g of the leaves, followed by vacuum filtration using Whatman No.3 filter paper. The three different concentrations of leaves extract prepared were used to synthesize three different ZnO NPs.

2.3.2. Preparation of ZnO using aqueous leaf extract of Coffea liberica

1 g of $Zn(NO_3)_2 \cdot 6H_2O$ was added to 50 mL of aqueous leaf extract and the solution was heated at

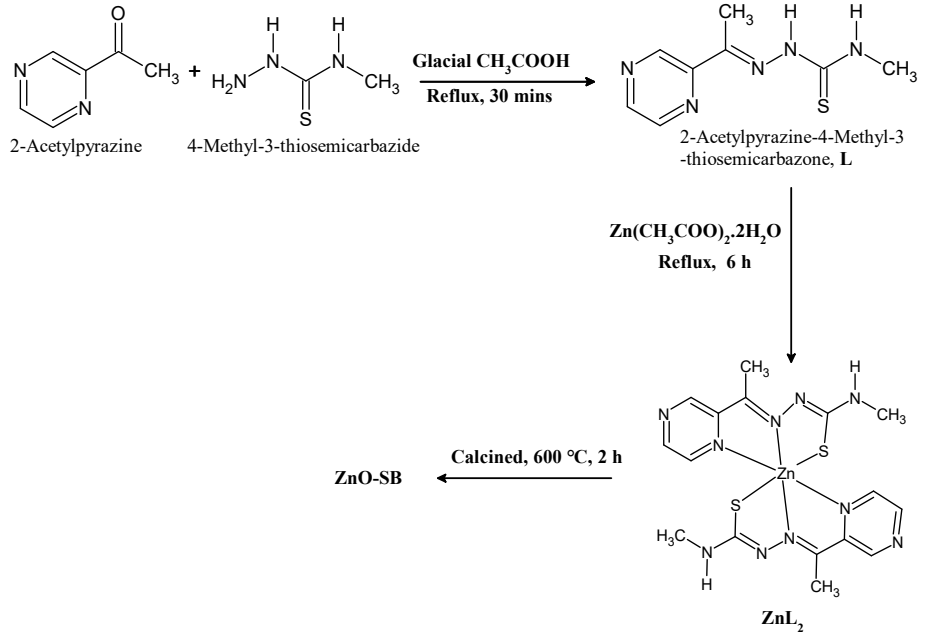

Fig. 1. Schematic diagram of chemical synthesis of ZnO NPs via Zn(II) Schiff base complex.

80 °C with stirring for 2 h until a formation of dark brown paste formed. The paste was then transferred into a crucible and calcined in a furnace at 600 °C for 2 h. The product was left to cool to room temperature before being ground finely using a pestle and mortar. The three synthesized ZnO were labelled as ZnO-1, ZnO-5, and ZnO-10 according to the amount of leaf powder used: 1 g, 5 g, and 10 g, respectively [27]. The summary of the procedure of green synthesized ZnO NPs is shown in Fig. 2.

2.4. Catalytic reaction

A mixture of 5 mmol of phenol and 5 mmol of benzoyl chloride was transferred into a 25 mL round bottom flask. 10 mol% ZnO (0.040 g) was added and stirred at room temperature until solidified, which took approximately two to 3 min. TLC was used to monitor the progress of the reaction. On completion of the reaction, CH_2Cl_2 (2 × 5 mL) was added to the mixture. The resulting mixture was filtered to remove the ZnO solid. The filtrate was then washed with 10 mL of 10 % aqueous $NaHCO_3$ and transferred into a 100 mL separating funnel. The two layers, consisting of the aqueous and organic layers, were collected in a separate beaker. The aqueous layer was extracted again with another 10 mL of CH_2Cl_2. The organic layers were then combined and dried with anhydrous Na_2SO_4. After 15 mins, the solution was filtered into a 50 mL round bottom flask and then rotary evaporated to obtain the phenyl benzoate as a white solid product. This procedure was done in triplicate for ZnO-SB, ZnO-1, ZnO-5, ZnO-10, and commercial ZnO (ZnO-C), and the average yield of product formed from the reaction was taken [7]. ZnO-5 gave the best yield for acylation and therefore was further studied as a catalyst for other phenol derivatives, which are 2-naphthol and 4-chlorophenol. Furthermore, as a control, the acylation reaction of phenol with benzoyl chloride with no catalyst was conducted, and there was no reaction. The recyclability of phenol using ZnO-5 was also carried out using the same conditions and procedure.

3. Results and discussion

3.1. Synthesis and characterization of L and ZnL_2

The syntheses and spectroscopic characterization of Schiff base ligand 2-acetylpyrazine-4-methyl

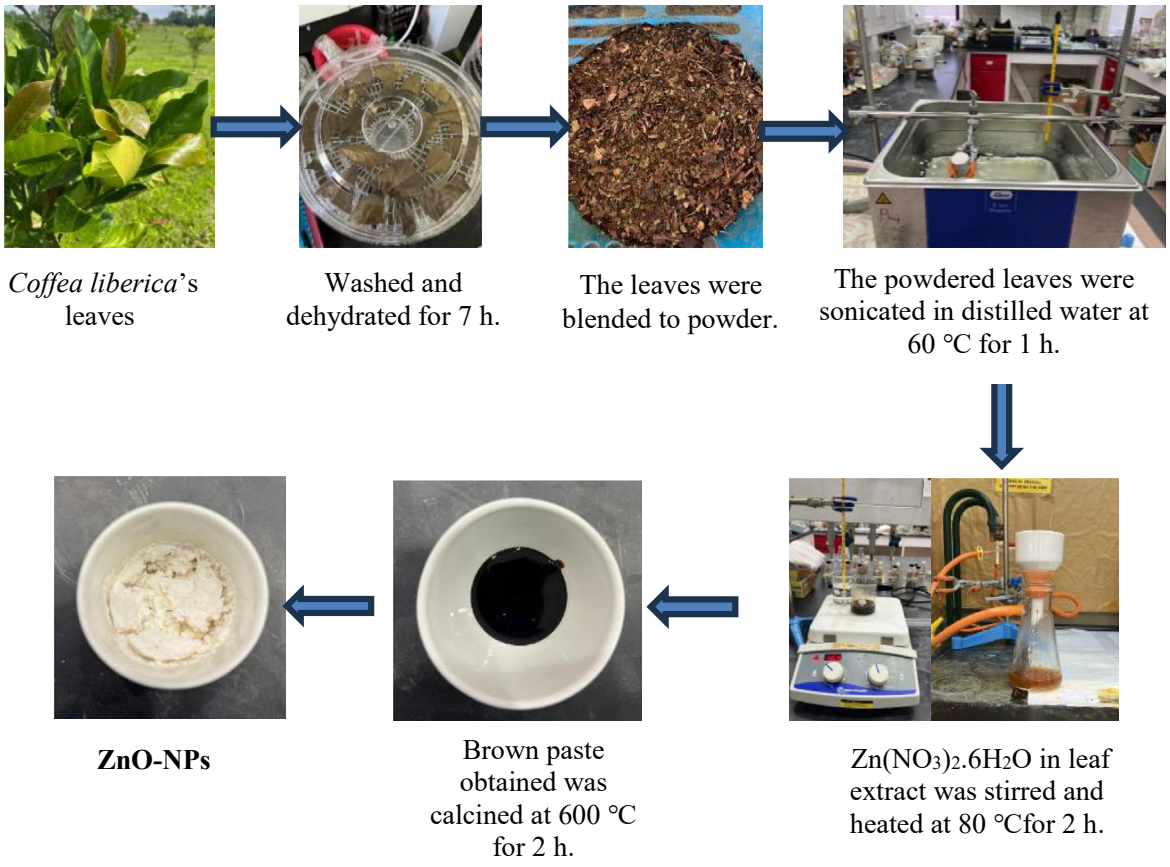

Fig. 2. Schematic diagram of green synthesis of ZnO NPs using Coffea liberica *leaf extract.*

thiosemicarbazone, abbreviated as L, have been previously reported in the literature [19]. The Schiff base ligand is commonly known for its functional group of thioamides, -NH-(C=S)-, thus they can exhibit thione-thiol tautomerism. The prepared Schiff base ligand, L, therefore, is likely to exist either as the thione or thiol tautomeric forms as shown in Fig. 3. However, the FTIR spectrum of L displays a ν(N—H) stretching band at 3302–3213 cm^{-1}, indicating that it adopts the thione tautomeric form in the solid state. This is further supported by the presence of ν(C=S) stretch in the ligand, which was detected at *ca.* 840 $cm^{-1,}$ and the absence of a ν(S—H) at *ca.* 2600–2500 cm^{-1}. The reaction with zinc(II) acetate dihydrate salt was performed by heating the mixture with a 1:2 metal-to-ligand ratio on a steam bath. The addition of the methanolic solution of metal salt to the Schiff base ligand, L, dissolved in hot acetonitrile, led to the formation of ZnL_2, an orange powder product (yield: 30 %). The Zn(II) complex obtained was found to be stable at room temperature and can be kept in a desiccator over anhydrous silica gel without any sign of decomposition. They are insoluble in most common organic solvents but soluble in DMF and DMSO. FTIR and UV-Vis spectroscopic techniques characterized the obtained compounds.

The selected FTIR spectrum ligand and complex, together with their assignments, and electronic spectra, are listed in Table 1. The ligand indicated the imine group ν(C=N) at the FTIR stretch at 1607 cm^{-1} is shifted to 1577 for the complex, which shows a clear indication of the coordination via the imine nitrogen atom. The data from the literature gives a result for the ligand that the ν(C=N) is 1610 cm^{-1} [28,29]. The band at 840 cm^{-1} in L is assigned to ν(C=S), whereas in its complex, the band shifted to a lower frequency, which is 821 cm^{-1}. The complex of Fe(II) shows similar results of the band shift for the complex from 837 to 829 cm^{-1} [29]. This shift indicates a successful coordination of sulfur [30]. Moreover, the free ligand and complex did not show ν(S-H) bonds at 2500-2600 cm^{-1}, indicating that the L and ZnL_2 in the solid state remain in the thione form [30]. The UV-Vis absorption was recorded using DMSO in the UV-Vis region (300–800 nm). The ligand L presented a band at 250 nm, which corresponds to the $n \rightarrow \pi^*$ transition, and a strong band at 328 nm, which can be assigned to the $\pi \rightarrow \pi^*$ transition. This transition closely aligns with previously reported values of 258 nm and 330 nm, reinforcing the electronic behavior of the free ligand [18]. Upon complexation with Zn(II), as displayed in Fig. 4, the absorption peaks are associated with the $n \rightarrow \pi^*$ transition and $\pi \rightarrow \pi^*$ transition, shifting to lower wavelengths at 248 nm and 322 nm, respectively. Additionally, the appearance of a distinct band at 421 nm, assigned to the MLCT transition, suggests that the formation of a metal complex occurred. Although

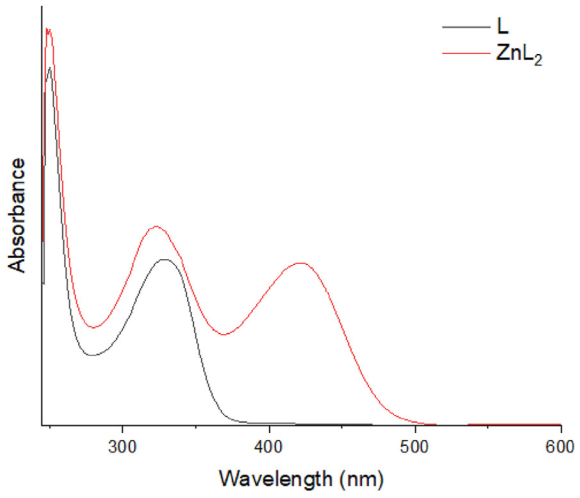

Fig. 4. Electronic Spectra of Ligand, L (black line) and zinc(II) complex, ZnL_2 (red line).

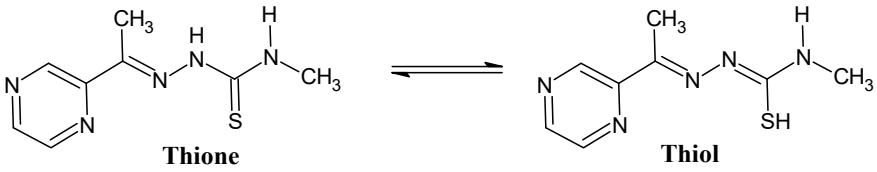

Fig. 3. Thione/Thiol tautomerism of Schiff base ligand, L.

Table 1. Selected FTIR vibration frequencies (cm^{-1}) for selected bonds in the ligand and complex and their electronic spectral data.

Compound	IR			UV-Vis spectra in DMSO λ_{max}/nm (Calc. molar absorptivity, Σ)
	ν(NH)	ν(C=N)	ν(C=S)	
L	3303, 3213	1607	840	250 (64,342), 328 (29,847)
ZnL_2	3260	1577	821	248 (165,283), 322 (82,613), 421 (67,624)

there is no literature report on the Zn(II) complex derived from L, similar trends have been observed in SB complexes of this ligand, L with other transition metals, such as Cd(II) and Sb(II), have been reported whereby MLCT bands were observed in the range of 400–450 nm [18]. This similarity supports the successful formation of the metal complex and the occurrence of metal-ligand coordination. The mass spectrum of L exhibits a peak at 210.10 *m/z*, corresponding to the [M+H] ion, which is consistent with its calculated molecular weight of 209.28. Similarly, ZnL_2 shows a molecular ion peak at *m/z* 481.10, attributed to the [M+H] ion, confirming its molecular mass of 481.92 as well as the confirmed deprotonation of the hydrogen attached to the nitrogen atom. These mass spectral findings, together with the elemental analysis, support the successful formation of Zn(II) complex with a general stoichiometry of [ZnL_2] in a ratio of 1:2. The elemental analyses indicated that ZnL_2 was formed with a 1:2 ratio.

3.2. FTIR analysis of the synthesized ZnO NPs

The synthesized ZnO NPs (ZnO-SB, ZnO-1, ZnO-5, and ZnO-10) from both chemical and green synthesis were all examined using FTIR spectroscopy in the range of 4000–400 cm^{-1}, as shown in Fig. 5 and compared to the ZnO-C. This analysis was used to determine the functional groups responsible for the reduction and stabilization of the synthesized NPs and functional

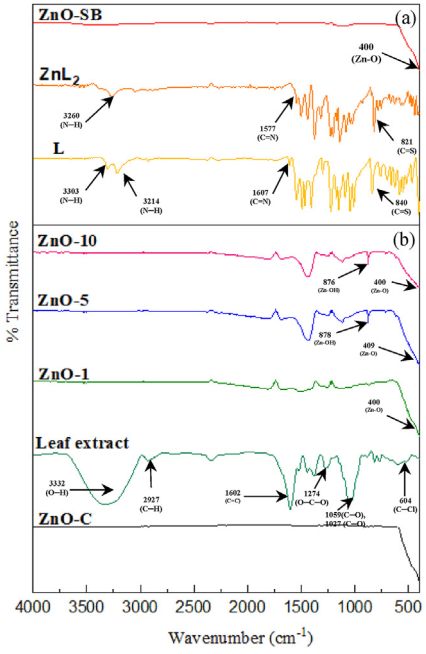

Fig. 5. FTIR spectra of ZnO NPs synthesized from (a) Chemical synthesis and (b) Green synthesis and ZnO-C.

groups present in L, ZnL2, and leaf extract. FTIR spectrum for the leaf extract showed a broad peak at 3332 cm^{-1}, which likely belongs to the *ν*(O–H) vibrations, indicative of the hydroxyl group of polyphenols. A strong absorption peak at 1602 cm^{-1} confirmed the presence of *ν*(C=C) stretch, suggesting the presence of phenolic compounds, flavonoids, or tannins. The absorption at 2927 cm^{-1} and 1444 cm^{-1} corresponds to *ν*(C–H) stretching of methyl or methylene group and the appearance of bending absorption of a methyl group at 1381 cm^{-1}, possibly linked to terpenoids or polysaccharides. The appearance of bending absorption of the *ν*(N–H) or aromatic *ν*(C=C) at 1523 cm^{-1} is potentially from proteins or alkaloids. The peaks attributed at 604 cm-1 indicate the presence of alkyl halides *ν*(C-Cl) [31]. Chlorogenic acid typically exhibits absorption in the range of approximately 1100–1300 cm^{-1} [32]. Moreover, acidic compounds such as chlorogenic acid, citric acid, and caffeic acid are characterized by distinct functional group absorptions including *ν*(C–O), *ν*(O–H), and *ν*(C–O–C) stretching vibrations which appear at approximately 1000–1100 cm^{-1}, 3000 cm^{-1}, and 1200 cm^{-1} respectively [33]. Additional peaks observed in the leaf extract at 1027 cm^{-1} and 1059 cm^{-1} are attributed to the presence of *ν*(C–O) which are likely due to the presence of chlorogenic acids, while the peak at 1275 cm-1 corresponds to the presence of *ν*(C–O–C) suggesting the presence of caffeic acid. This confirmed the presence of phytochemicals such as alkaloids, such as caffeine, flavonoids, polyphenols, and phenolics such as catechins and tannins [23]. Based on the FTIR spectra, medium intense bands of Zn-O stretching were observed at approximately 400 cm^{-1} for ZnO-SB, ZnO-1, ZnO-10, and ZnO-C, while 409 cm^{-1} for ZnO-5. Moreover, Zn-OH peaks were observed at approximately 878 cm^{-1} for ZnO-5 and ZnO-10. There is a significant difference that can be observed between green synthesized ZnO NPs and chemically synthesized ZnO NPs and ZnO-C. The intensity of the absorption bands associated with the organic molecules increases in correlation with the higher concentration of leaf extract used in the production of ZnO NPs. This is attributed to the abundance of phytochemicals in the more concentrated extract [26,34]. As anticipated, the absence of these bands in the FTIR spectrum of the ZnO-C confirms the presence of phytochemicals on the surfaces of all green synthesized ZnO NPs. As a result, this demonstrates that the green synthesis method can be employed to prepare ZnO NPs and the possibility for organic elements to be incorporated into their structure [35]. In contrast, the ZnO-SB from chemical synthesis shows no such peaks, confirming complete thermal decomposition to give ZnO NPs without surface-bound organic compounds. This comparison highlights how green synthesis can

offer additional benefits, such as functionalized surfaces which may be an advantage for their applications.

3.3. X-ray diffraction analysis

XRD was used to determine the crystallographic nature and atomic structure of materials. Fig. 6 exhibits the XRD pattern of ZnO-SB, ZnO-1, ZnO-5, and ZnO-10 were indexed to (100), (002), (101), (102), (110), (103), (200), (112) and (201) planes of hexagonal wurtzite structure which correspond to 2θ values of 31.84°, 34.50°, 36.34°, 47.65°, 56.73°, 63.02°, 66.54°, 68.12° and 69.26°, respectively. XRD patterns matched with the ZnO standard diffraction pattern obtained from the Joint Committee on Powder Diffraction Standards (JCPD ZnO 01-075-0576), which confirms that the synthesized ZnO NPs possess a hexagonal wurtzite phase, aligning with the X-ray diffraction results. The sharp peaks presented at (100), (002), and (101) denote high crystalline and single-phase ZnO NPs. ZnO-5 and ZnO-10 show an extra peak attributed to (001), and this is believed to be due to their lattice strain and interplanar spacing [36]. These findings correlate with the result obtained by Wang et al. [26]. The average crystallite sizes of all the synthesized ZnO NPs were calculated using the Debye-Scherrer Equation [1]:

$$D = \frac{0.94\lambda}{\beta \cos\theta} \quad (1)$$

where D is the crystallite size, λ is the wavelength of Cu Kα radiation (1.54060 Å) and β is the full width at half maximum (FWHM) in radians and θ is the Bragg diffraction angle. The average crystallite size and lattice parameters of a and c were identified by analyzing the three most intense peaks which correspond to the (100), (002), and (101) in the XRD pattern. The symbols a and c are denoted as the lattice parameters, Furthermore, the unit cell volume of the NPs was calculated using Equation [2]:

$$V = \frac{\sqrt{3}}{2} a^2 c \quad (2)$$

Table 2 shows the calculated lattice parameters a and c, the average crystallite size, and the unit cell volume, V(Å)^3 for all the samples. The average crystallite size of green synthesized ZnO NPs ranges from 29.47 to 58.12 nm. The results show that the green synthesized ZnO NPs exhibited an increase in crystallized size as the concentration of extract used for the synthesis increases. A similar observation was reported for ZnO NPs synthesized from *Coffea arabica* leaf with masses of 10 g, 15 g, 20 g, and 25 g [25]. ZnO-5 has the largest average crystallite size at 58.47 nm, compared to ZnO-1 (29.47 nm) and ZnO-10 (37.46 nm). Interestingly, the chemical synthesized ZnO-SB gave an even smaller crystallite size of 23.17 nm than the green synthesized ZnO NPs. Paul et al. [14] reported that the calculated crystallite size of its ZnO NPs derived from Zn(II) complex shows a bigger value (36.2 nm) than our compound.

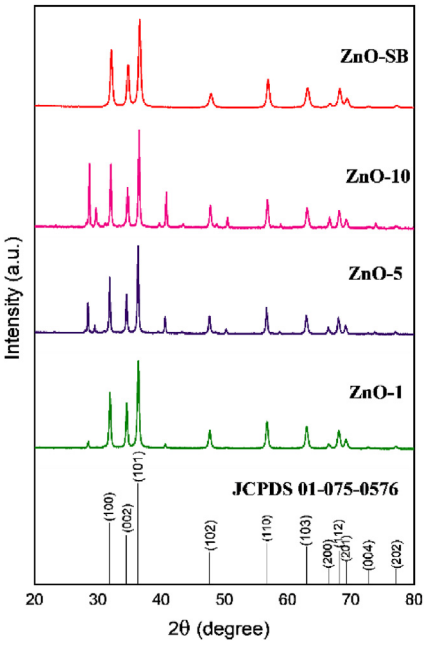

Fig. 6. XRD results of synthesized ZnO NPs.

3.4. Scanning electron microscopy and energy-dispersive X-ray spectroscopy

The morphological characteristics and the particle size of all the synthesized ZnO NPs (ZnO-SB, ZnO-1, ZnO-5, and ZnO-10) were analyzed using the SEM technique. Both SEM and EDX images of these nanoparticles are presented in Fig. 7. The results show that the green synthesized ZnO NPs are more porous than chemically synthesized ZnO NPs. The SEM micrograph of ZnO-SB presents a mixture of both irregular and spherical-shaped particles, and they are densely packed

Table 2. Structural lattice parameters, a and c (Å), the average crystallite size (nm) and unit cell volumes (Å)^3 obtained from XRD patterns of ZnO NPs synthesized using a different mass of leaves and Zn(II) complex as a precursor.

Samples	Lattice parameters		Average crystallite size (nm)	Unit cell volume V(Å)^3
	a (Å)	*c* (Å)		
ZnO-SB	3.22	5.16	23.17	46.34
ZnO-1	3.24	5.19	29.47	47.24
ZnO-5	3.24	5.19	58.12	47.31
ZnO-10	3.23	5.17	37.46	46.72

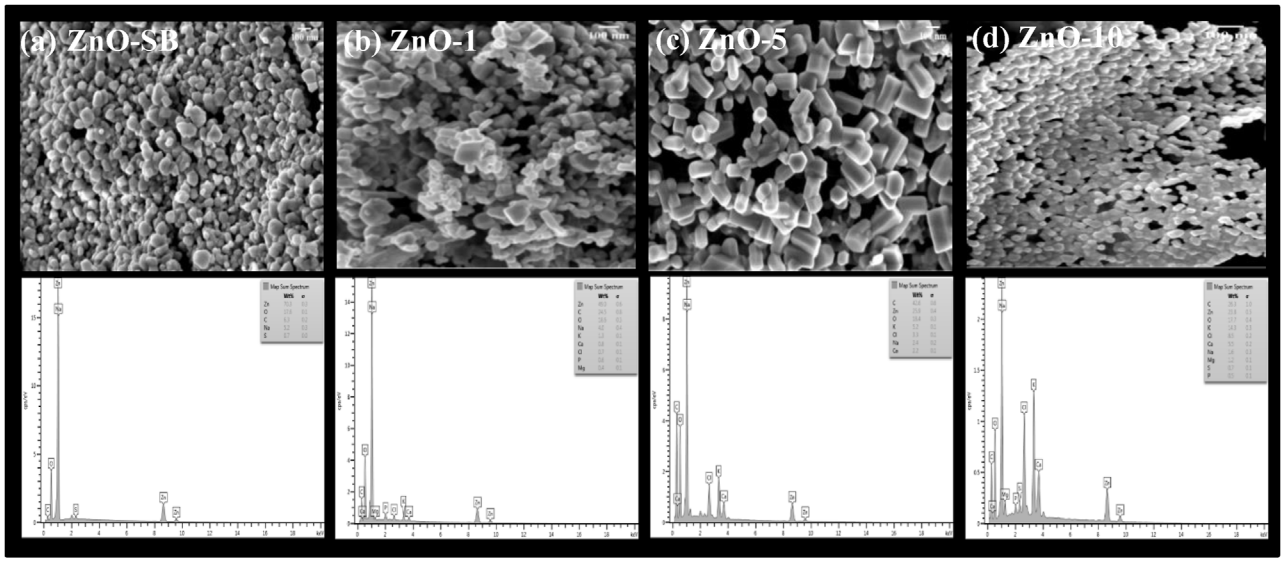

Fig. 7. SEM image and EDX spectrum of synthesized ZnO NPs: (a) ZnO-SB, (b) ZnO-1, (c) ZnO-5, and (d) ZnO-10 at ×50,000 magnification.

together (Fig. 7a). The morphology of ZnO-1, synthesized from a lower concentration of *Coffea liberica* extract displayed in Fig. 7b appears as agglomerated clusters with irregular and spherical shaped particles. Agglomeration of particles is due to the hydrogen bonding and electrostatic interaction between bio-organic capping molecules and NPs [37]. The SEM characterization of ZnO-5 reveals surface porosity containing more defined and rod-like structured particles (Fig. 7c). ZnO-10 shows a densely packed morphology with a mixture of both irregular-shaped particles (Fig. 7d) [34]. The densely packed and less porous surface observed for ZnO-10 could be due to the high concentration of leaf extract used for the fabrication of ZnO NPs which leads to a higher quantity of phytochemicals being present. This shape variation indicates that the higher extract concentration might affect the particle formation and surface characteristics. Table 3 shows the average particle size calculated for all synthesized ZnO NPs using ImageJ software. The results show that amongst the synthesized NPs, ZnO-SB has the largest average particle size of 51.80 nm, followed by ZnO-1, ZnO-5, and ZnO-10 with 42.18, 40.56 nm and 34.34 nm, respectively. The particle size of green synthesized ZnO decreases with an increasing concentration of leaf extract used in the synthesis, which could be attributed to the higher amount of phytochemicals present. A similar trend has been reported by Abel et al. [25] using different masses of *Coffea arabica* leaf extract 10 g, 15 g, 20 g, and 25 g resulting in a decrease in size from 10 μm, 5 μm, 2 μm, and 1 μm, respectively. Another study also shows a similar trend whereby as the concentration of *Citrus microcarpa* (calamansi) peel extract used for the synthesis of ZnO was increased from 1 % to 2 % and 4 %, a decrease in the nanoparticle size from 39.7 nm to 16.8, and 13.1 nm, respectively [34]. Soto-Robles et al. [38] synthesized ZnO NPs with varying concentrations of *Hibiscus sabdariffa* extract (1 %, 4 %, and 8 %) and they determined that ZnO synthesized with 8 % extract presented the smallest particle size with sizes ranging from 5 to 12 nm, while ZnO synthesized with 1 % extract presented the largest particle size that ranges from 20 to 40 nm. These reports confirmed that the concentration of extract used in ZnO NPs synthesis plays a crucial role in determining the particle size of the NPs. A similar observation was reported, where a higher concentration of *Hibiscus sabdariffa* flower extract resulted in more extensive material coverage [38]. The EDX spectra confirmed the presence of zinc, and oxygen in all synthesized ZnO NPs; a few other low-intensity peaks were also observed in the EDX spectra. For chemical synthesis, very low intensity of other peaks such as carbon and sulfur, while green synthesized ZnO NPs indicate the presence of the peak for elements such as carbon and potassium which could have originated from the leaf extract; hence it shows that these phytochemicals from the leaf extract are involved in the reduction and capping of ZnO [39].

Table 3. The average particle morphology and size of all synthesized ZnO NPs in nm.

Samples	Particle size in nm
ZnO-SB	51.80
ZnO-1	42.18
ZnO-5	40.56
ZnO-10	34.34

3.5. Catalytic reaction for the acylation of phenol

The catalytic activity of the synthesized ZnO NPs (ZnO-SB, ZnO-1, ZnO-5, and ZnO-10) was evaluated in the acylation of phenol using benzoyl chloride under solvent-free conditions at room temperature. Additionally, the catalytic efficiency of these ZnO NPs was compared to that of ZnO-C used as a catalyst. The proposed mechanism of ZnO NPs in the acylation reaction of alcohols and phenols is shown in Scheme 1 [40]. The acylation of phenol with benzoyl chloride, catalyzed by synthesized ZnO NPs and ZnO-C, successfully produced phenyl benzoate (Scheme 2). The results are summarized in Table 4 and depicted in Fig. 8. The catalytic performance varied depending on the source of ZnO NPs. ZnO-SB demonstrated a slightly lower yield of 50 % in 2 minutes but produced a product with a higher melting point range of 68–70 °C. Meanwhile, ZnO-C and ZnO-1 achieved similar yields (60 %) with reaction times of 2 and 3 minutes, respectively, which is lower than the results obtained by Hosseini Sarvari and Shargi (95%) [7]. However, the reaction time is much faster than the reported time of 30 minutes [7]. Among the ZnO NPs derived from *Coffea liberica* leaf extracts, ZnO-5 showed the best performance, yielding 63 % of the product in 3 minutes with a melting point of 68–70 °C. In comparison, ZnO-10 has the lowest yield (55 %) while maintaining a melting point range of 65–68 °C. The melting points of the product in this study ranged between 65 and 70 °C, closely aligning with the literature-reported melting point (68–70 °C) [41]. This consistency in melting point verifies the products' purity and supports the target compound's successful formation. Further analysis using FTIR shows that the peaks of ν(C=O) are close (1726 cm^{-1}) to their reported peak (1729 cm^{-1}) [42].

Table 4. The acylation reaction of phenol and benzoyl chloride using synthesized ZnO NPs.

Catalyst	Time (mins)	Average Yield (%)	Melting point of product/°C
ZnO-C	2	60(2)	65–68
ZnO-SB	2	50(3)	68–70
ZnO-1	3	60(2)	65–70
ZnO-5	3	63(2)	68–70
ZnO-10	3	55(3)	65–68

The differences in catalytic efficiency among the synthesized ZnO NPs can be attributed to variations in NPs size, surface area, and morphology, as influenced by the synthesis methods and precursor concentration, as shown in Fig. 7 and Table 2. These findings highlight that green synthesized ZnO NPs, particularly ZnO-5, can outperform ZnO-C under specific conditions, making them a promising green alternative for catalytic applications. The higher catalytic performance of ZnO-5 could be attributed to their nanorod-like structure and high porous morphology is due to their combined framework and textural porosity, which increases the interaction of reactants with active sites and reduces diffusion limitation [43]. ZnO-SB demonstrates that SB-derived ZnO NPs catalysts may have unique properties that influence catalytic outcomes. This underscores the significance of precursor materials and synthesis strategies in catalyst design from their densely packed morphology.

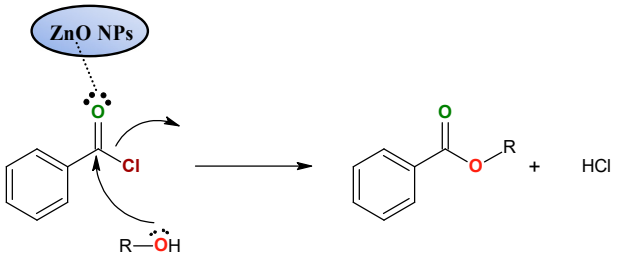

Scheme 1. Proposed mechanism of ZnO NPs in the acylation reaction of alcohol and phenols [40].

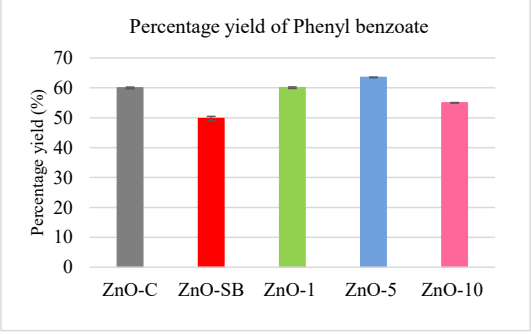

Fig. 8. The percentage yield of phenyl benzoate was obtained using 10 mol % of all synthesized ZnO NPs and ZnO-C as the catalyst.

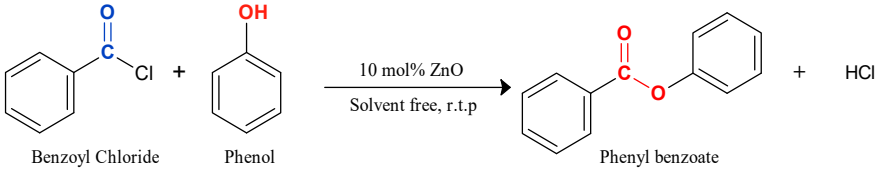

Scheme 2. Acylation of phenol using ZnO catalyst.

Table 5. The acylation reaction of phenol derivatives using ZnO-5.

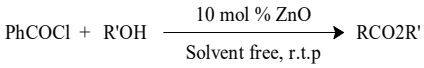

Entry	Substrate name	Substrate structure	Time (mins)	Average Yield (%)	Melting point (°C)
1	Phenol	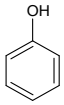	3	63	68–70
2	2-Naphthol	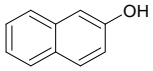	5	68	105–108
3	4-Chlorophenol	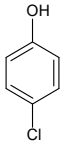	2	64	86–90

Based on the high performance of ZnO-5, further experiments were carried out on two other derivatives with benzoyl chlorides, such as 2-naphthol and 4-chlorophenol. Table 5 displays the results of the three substrates—phenol, 2-naphthol, and 4-chlorophenol, yielding distinct results in terms of reaction time, product yield, and melting points. Among the substrates, 2-naphthol (entry 2) exhibited the highest average product yield of 68 % with a reaction time of 5 minutes, indicating higher reactivity as compared to phenol and 4-chlorophenol (entries 1 and 3). This could be due to the bulky and more planar aromatic system of 2-naphthol that reduces steric hindrance for reactivity [44]. 4-chlorophenol showed better reactivity than phenol due to the presence of a chlorine substituent at the para position, which is an electron-withdrawing group that stabilized the phenoxide ion during the acylation reaction [45]. 2-naphthyl benzoate demonstrated a melting point range of 105–108 °C which is in agreement with the melting point reported in literature [46]. The catalytic reaction of entry 1 required 3 minutes and yielded 63 % of the product, while with entry 3, a slightly higher yield of product was obtained. The melting point of 4-chlorophenyl benzoate obtained at 86–90 °C is the same as reported in the literature [47]. In addition, FTIR was also obtained to confirm the peaks of the ester present for both phenol derivatives [48,49]. The differences in yields and reaction times highlight the influence of the substrate on the reaction efficiency, with entry 2 benefiting from its extended aromatic system and increased nucleophilicity. This study underscores the potential of ZnO NPs as effective catalysts for environmentally friendly, rapid, and efficient acylation reactions.

The recyclability of a catalyst is a key indicator of its performance and sustainability in catalytic processes. In this study, we investigated the reusability of ZnO-5 on a model reaction of phenol and benzoyl chloride under similar experimental conditions. This esterification allows for a straightforward assessment of catalyst activity and durability over successive uses. The results, as summarized in Table 6 revealed that the ZnO-5 catalyst was reused up to three times without significant loss of catalytic efficiency. This recyclability highlights the catalyst potential for sustainable applications, reducing waste and operational costs in industrial processes. Furthermore, the ability of the ZnO-5 catalyst to retain activity over multiple cycles underscores its sustainability for long-term use in esterification and related transformations, supporting its viability in environmentally conscious chemical applications.

Table 6. Recyclability study of ZnO-5 for acylation of phenol with benzoyl chloride.

Run	1	2	3	4
Time (mins)	3	3	8	12
Yield (%)	63.5	63.4	62.1	57.8

4. Conclusions

ZnO NPs were successfully synthesized via chemical and green methods. The chemical synthesis of ZnO NPs was derived from the thermal decomposition of zinc(II) 2-acetylpyrazine-4-methylthiosemicarbazone, ZnL_2 as a precursor, whilst the green synthesis of ZnO NPs was derived using *Coffea liberica* leaves extract with three different masses (1 g, 5 g, and 10 g) as a reducing and capping agent. The synthesis of zinc(II) 2-acetylpyrazine-4-methylthiosemicarbazone was successfully achieved by a 1:2 M ratio of metal(II) salt and ligand and ZnL_2 has been fully characterized. The spectroscopic data confirmed NNS tridentate coordination of the ligand with the metal ion. The XRD

crystallite sizes for ZnO-SB, ZnO-1, ZnO-5, and ZnO-10 are calculated to be 23.17 nm, 29.47 nm, 58.12 nm, and 37.46 nm, respectively. SEM images displayed interesting rodlike structures with high porosity for ZnO-5, while ZnO-1, ZnO-10, and ZnO-SB show irregular and spherical structures with less porous morphology. The average particle sizes of ZnO-1, ZnO-5, ZnO-10, and ZnO-SB were calculated to be 42.18 nm, 40.56 nm, 34.34 nm, and 51.80 nm, respectively. It was observed that the average particle size of the green synthesized ZnO NPs decreases with increasing concentration of the extract used for the synthesis. The catalytic activity of the acylation reaction of phenol with benzoyl chloride was also successfully carried out with all the synthesized ZnO NPs as catalysts, and the finding demonstrated that ZnO-5 produced a higher yield of phenyl benzoate as compared to other synthesized ZnO-NPs and ZnO-C. This remarkable catalytic performance can be attributed to the unique rodlike and highly porous morphology, favorable crystallite size, and reduced agglomeration, which enhances the surface area and provides a stable, highly reactive surface for the reaction. ZnO-5 was used for the catalytic studies in the acylation reactions of 2-naphthol and 4-chlorophenol, where the acylation product of 2-naphthol shows a higher yield (68 %) than phenol (63 %) and 4-chlorophenol (64 %) substrates. The reusability of the acylation of phenol using ZnO-5 was also carried out under similar conditions. The catalyst showed excellent recoverability and reusability over three successive runs under the same conditions. Our results confirm the potential use of green synthesized ZnO NPs from *Coffea liberica* leaf as a catalyst in a simple organic reaction.

Funding

Funding was provided by UBD Faculty Research Grants (award No. UBD/RSCH/1.4/FICBF(b)/2020/024 and UBD/RSCH/1.4/FICBF/2024/075).

Conflict of interest

The authors have no relevant financial or non-financial interests to disclose.

Acknowledgment(s)

This work was supported by Universiti Brunei Darussalam Research grant UBD/RSCH/1.4/FICBF(b)/2020/024 and UBD/RSCH/1.4/FICBF/2024/075. We are grateful for the support of the Chemical Sciences, Faculty of Science at Universiti Brunei Darussalam for extending their facilities for some analyses (FTIR, XRD, UV-Vis) and UKM for conducting SEM-EDX and CHN analyses, and the National University of Singapore (NUS) for running the MS spectroscopy analysis. We would also like to express our sincere gratitude to Labi Farm, Brunei Darussalam, for providing the *Coffea liberica* leaves used in this study.

References

[1] O.R. Brown, D.A. Hullender, Biological evolution requires an emergent, self-organizing principle, Prog. Biophys. Mol. Biol. 182 (2023) 75−102, https://doi.org/10.1016/j.pbiomolbio.2023.06.001.

[2] K.M. Manoj, V.D. Jacob, M. Kavdia, H. Tamagawa, L. Jaeken, V. Soman, Questioning physiological rotary functionality in the bacterial flagellar system and proposing a murburn model for motility, 2023.

[3] T.F.S. Silva, L.M.D.R.S. Martins, Recent advances in copper catalyzed alcohol oxidation in homogeneous medium, Molecules 25 (2020), https://doi.org/10.3390/molecules25030748.

[4] F. Lu, D. Astruc, Nanocatalysts and other nanomaterials for water remediation from organic pollutants, Coord. Chem. Rev. 408 (2020), https://doi.org/10.1016/j.ccr.2020.213180.

[5] S. Ullah, M. Shaban, A.B. Siddique, A. Zulfiqar, N.S. Lali, M. Naeem-ul-Hassan, et al., Greenly synthesized zinc oxide nanoparticles: an efficient, cost-effective catalyst for dehydrogenation of formic acid and with improved antioxidant and phyto-toxic properties, J. Environ. Chem. Eng. 12 (2024), https://doi.org/10.1016/j.jece.2024.113350.

[6] M.M.A. Soliman, A. Karmakar, E.C.B.A. Alegria, A.P.C. Ribeir, G.M. D.M. Rúbio, M.S. Saraiva, et al., ZnO nanoparticles: an efficient catalyst for transesterification reaction of α-keto carboxylic esters, Catal. Today 348 (2020) 72−79, https://doi.org/10.1016/j.cattod.2019.08.053.

[7] M. Hosseini Sarvari, H. Sharghi, Zinc oxide (ZnO) as a new, highly efficient, and reusable catalyst for acylation of alcohols, phenols and amines under solvent free conditions, Tetrahedron 61 (2005) 10903−10907, https://doi.org/10.1016/j.tet.2005.09.002.

[8] F. Tamaddon, M.A. Amrollahi, L. Sharafat, A green protocol for chemoselective O-acylation in the presence of zinc oxide as a heterogeneous, reusable and eco-friendly catalyst, Tetrahedron Lett. 46 (2005) 7841−7844, https://doi.org/10.1016/j.tetlet.2005.09.005.

[9] S. Kuld, M. Thorhauge, H. Falsig, C.F. Elkjær, S. Helveg, I. Chorkendorff, et al., Quantifying the promotion of Cu catalysts by ZnO for methanol synthesis, Science (1979) 352 (2016) 969−974, https://doi.org/10.1126/science.aaf0718.

[10] P.C. Nagajyothi, T.N. Minh An, T.V.M. Sreekanth, J Il Lee, D.L. Joo, K.D. Lee, Green route biosynthesis: characterization and catalytic activity of ZnO nanoparticles, Mater. Lett. 108 (2013) 160−163, https://doi.org/10.1016/j.matlet.2013.06.095.

[11] A. Rahmatpour, Polystyrene-supported GaCl 3: a new, highly efficient and recyclable heterogeneous lewis acid catalyst for acetylation and benzoylation of alcohols and phenols, C. R. Chim. 15 (2012) 1048−1054, https://doi.org/10.1016/j.crci.2012.08.005.

[12] Y. Barot, S. Mishra, V. Anand, R. Mishra, Iron containing dicationic ionic liquid [DIL]2+[2FeCl4]2− as a highly efficient catalyst for the acylation of alcohols, phenols and amines, Catal. Commun. 182 (2023), https://doi.org/10.1016/j.catcom.2023.106739.

[13] P.K. Mishra, H. Mishra, A. Ekielski, S. Talegaonkar, B. Vaidya, Zinc oxide nanoparticles: a promising nanomaterial for biomedical applications, Drug Discov. Today 22 (2017) 1825−1834, https://doi.org/10.1016/j.drudis.2017.08.006.

[14] S. Paul, H.P. Gogoi, A. Singh, P. Barman, Nanostructured metal oxides by facile thermal decomposition of Zinc(II) and Copper(II) schiff base complexes: microwave synthesis of complexes, characterization, DFT study, optical properties and application of its oxides in multicomponent biginelli reaction,

Inorg. Chem. Commun. 153 (2023), https://doi.org/10.1016/j.inoche.2023.110760.
[15] A.D. Khalaji, M. Nikookar, K. Fejfarova, M. Dusek, Synthesis of new cobalt(III) schiff base complex: a new precursor for preparation Co3O4 nanoparticles via solid-state thermal decomposition, J. Mol. Struct. 1071 (2014) 6–10, https://doi.org/10.1016/j.molstruc.2014.04.043.
[16] D. Mutukwa, R. Taziwa, L.E. Khotseng, A review of the green synthesis of ZnO nanoparticles utilising southern African Indigenous medicinal plants, Nanomaterials 12 (2022), https://doi.org/10.3390/nano12193456.
[17] J. Wang, Y.T. Wang, J.N. Chang, M.X. Li, Two nickel (II) complexes of 2-acetylpyrazine thiosemicarbazones: synthesis, crystal structures and biological evaluation, Inorg. Chem. Commun. 123 (2021), https://doi.org/10.1016/j.inoche.2020.108365.
[18] J. Wang, Z.M. Zhang, M.X. Li, Synthesis, characterization, and biological activity of cadmium (II) and antimony (III) complexes based on 2-acetylpyrazine thiosemicarbazones, Inorg. Chim. Acta. 530 (2022), https://doi.org/10.1016/j.ica.2021.120671.
[19] J. Zhou, Y.X. Wang, C.L. Chen, M.X. Li, 2-Acetylpyrazine 4-methylthiosemi-carbazone, Acta Crystallogr. Sect. E Struct. Rep. Online 64 (2008), https://doi.org/10.1107/S160053680706285X.
[20] M. Carlström, S.C. Larsson, Coffee consumption and reduced risk of developing type 2 diabetes: a systematic review with meta-analysis, Nutr. Rev. 76 (2018) 395–417, https://doi.org/10.1093/nutrit/nuy014.
[21] K.J. Cloete, Ž. Šmit, R. Minnis-Ndimba, P. Vavpetič, A. du Plessis, S.G. le Roux, et al., Physico-elemental analysis of roasted organic coffee beans from Ethiopia, Colombia, Honduras, and Mexico using X-ray micro-computed tomography and external beam particle induced X-ray emission, Food Chem. X 2 (2019), https://doi.org/10.1016/j.fochx.2019.100032.
[22] R.H. Cheney, A monograph of the economic species of the genus coffea L, 1925.
[23] D.L.J.M. Baay, R.V. Borromeo, F.C. Paglinawan, In vitro phytochemical screening, antioxidant activity and cytotoxicity of *Coffea liberica* ethanolic leaf extract, Int. J. Bot. Stud. 9 (2024) 31–35.
[24] N. Ostovar, N. Mohammadi, F. Khodadadeh, Photocatalytic, antioxidant and antibacterial potential of bio-synthesized ZnO nanoparticles derived from espresso spent coffee grounds: optimization by central composite design, Inorg. Nano-Met. Chem. 53 (2023) 938–949, https://doi.org/10.1080/24701556.2023.2187419.
[25] S. Abel, J.L. Tesfaye, R. Shanmugam, L.P. Dwarampudi, G. Lamessa, N. Nagaprasad, et al., Green synthesis and characterizations of zinc oxide (ZnO) nanoparticles using aqueous leaf extracts of coffee (Coffea arabica) and its application in environmental toxicity reduction, J. Nanomater. 2021 (2021), https://doi.org/10.1155/2021/3413350.
[26] Q. Wang, S. Mei, P. Manivel, H. Ma, X. Chen, Zinc oxide nanoparticles synthesized using coffee leaf extract assisted with ultrasound as nanocarriers for mangiferin, Curr. Res. Food Sci. 5 (2022) 868–877, https://doi.org/10.1016/j.crfs.2022.05.002.
[27] A.S. Abdelbaky, A.M.H.A. Mohamed, M. Sharaky, N.A. Mohamed, Y.M. Diab, Green approach for the synthesis of ZnO nanoparticles using Cymbopogon citratus aqueous leaf extract: characterization and evaluation of their biological activities, Chem. Biol. Technol. Agric. 10 (2023), https://doi.org/10.1186/s40538-023-00432-5.
[28] X. Feng Zhu, L. Zhi Zhang, M. Yang, Y. Ke Li, Li M. Xue, Synthesis, characterization, crystal structure, and cytotoxicity of a 7-Co-ordinate Diorganotin(IV) complex of 2-Acetylpyrazine N 4-Methylthiosemicarbazone, Z. Naturforsch. 67 (2012) 149–153.
[29] L.P. Zheng, C.L. Chen, J. Zhou, M.X. Li, Y.J. Wu, Synthesis, crystal structure and antitumor study of an Iron(III) complex of 2-Acetylpyrazine N(4)-Methylthiosemicarbazone, Z. Naturforsch. B Chem. Sci. 63 (2008) 1257–1261, https://doi.org/10.1515/znb-2008-1103.
[30] M.X. Li, C.L. Chen, C.S. Ling, J. Zhou, B.S. Ji, Y.J. Wu, et al., Cytotoxicity and structure-activity relationships of four α-N-heterocyclic thiosemicarbazone derivatives crystal structure of 2-acetylpyrazine thiosemicarbazone, Bioorg. Med. Chem. Lett. 19 (2009) 2704–2706, https://doi.org/10.1016/j.bmcl.2009.03.135.
[31] D. Ramimoghadam, MZ Bin Hussein, Y.H. Taufiq-Yap, The effect of sodium dodecyl sulfate (SDS) and cetyltrimethylammonium bromide (CTAB) on the properties of ZnO synthesized by hydrothermal method, Int. J. Mol. Sci. 13 (2012) 13275–13293, https://doi.org/10.3390/ijms131013275.
[32] C. Campa, R. Jean Jacques, A. De Kochko, C. Claudine, R.R. Jean-Jacques, Alexandre de Kochko, et al., Chlorogenic acids: diversity in green beans of wild coffee species, Adv. Plant Physiol. 10 (2008) 421–437.
[33] M. Latief, Heriyanti, I.L. Tarigan, Sutrisno, Preliminary data on the antibacterial activity of *Coffea arabica*, *Coffea canephora* and *Coffea liberica*, Pharmacogn. J. 14 (2022) 413–424, https://doi.org/10.5530/pj.2022.14.53.
[34] A. Villegas-Fuentes, H.E. Garrafa-Gálvez, R.V. Quevedo-Robles, M. Luque-Morales, A.R. Vilchis-Nestor, P.A. Luque, Synthesis of semiconductor ZnO nanoparticles using citrus microcarpa extract and the influence of concentration on their optical properties, J. Mol. Struct. 1281 (2023), https://doi.org/10.1016/j.molstruc.2023.135067.
[35] P.A. Luque, H.E. Garrafa-Gálvez, O. Nava, A. Olivas, M.E. Martínez-Rosas, A.R. Vilchis-Nestor, et al., Efficient sunlight and UV photocatalytic degradation of methyl orange, methylene blue and rhodamine B, using citrus×paradisi synthesized SnO2 semiconductor nanoparticles, Ceram. Int. 47 (2021) 23861–23874, https://doi.org/10.1016/j.ceramint.2021.05.094.
[36] P.K. Upadhyay, V.K. Jain, S. Sharma, A.K. Shrivastav, R. Sharma, Green and chemically synthesized ZnO nanoparticles: a comparative study, IOP Conf. Ser. Mater. Sci. Eng. 798 (2020), https://doi.org/10.1088/1757-899X/798/1/012025.
[37] F. Rahman, M.A. Majed Patwary, M.A. Bakar Siddique, M.S. Bashar, M.A. Haque, B. Akter, et al., Green synthesis of zinc oxide nanoparticles using *Cocos nucifera* leaf extract: characterization, antimicrobial, antioxidant and photocatalytic activity, R. Soc. Open Sci. 9 (2022), https://doi.org/10.1098/rsos.220858.
[38] C.A. Soto-Robles, P.A. Luque, C.M. Gómez-Gutiérrez, O. Nava, A.R. Vilchis-Nestor, E. Lugo-Medina, et al., Study on the effect of the concentration of *Hibiscus sabdariffa* extract on the green synthesis of ZnO nanoparticles, Results Phys. 15 (2019), https://doi.org/10.1016/j.rinp.2019.102807.
[39] A. Moezzi, A.M. McDonagh, M.B. Cortie, Zinc oxide particles: synthesis, properties and applications, Chem. Eng. J. 185–186 (2012) 1–22, https://doi.org/10.1016/j.cej.2012.01.076.
[40] Z. Mirjafary, H. Saeidian, A. Sadeghi, F.M. Moghaddam, ZnO nanoparticles: an efficient nanocatalyst for the synthesis of β-acetamido ketones/esters via a multi-component reaction, Catal. Commun. 9 (2008) 299–306, https://doi.org/10.1016/j.catcom.2007.06.018.
[41] Sigma Aldrich, Phenyl Benzoate SAFETY DATA SHEET, 2024.
[42] Chemical book, n.d. https://www.chemicalbook.com/SpectrumEN_93-99-2_IR1.htm (accessed 26, November, 2024).
[43] Y. Sun, L. Chen, Y. Bao, Y. Zhang, J. Wang, M. Fu, et al., The applications of morphology controlled ZnO in catalysis, Catalysts 6 (2016), https://doi.org/10.3390/catal6120188.
[44] Hai Truong Nguyen, Phuong Hoang Tran, An extremely efficient and green method for the acylation of secondary alcohols, Phenols and Naphthols with Deep Eutectic Solvent as Catalyst, Royal Society of Chemistry, 2016, https://doi.org/10.1039/C6RA22757K.
[45] A.K. Chandra, T. Uchimaru, The O-H bond dissociation energies of substituted phenols and proton affinities of substituted phenoxide ions: a DFT study, Int. J. Mol. Sci. 3 (2002) 407–422.
[46] ThermoFisher scientific, 2-Napthyl benzoate, SDS, 2021.
[47] TCI, 4-Chlorophenyl ester, SDS, 2018.
[48] Chemical book 2-Naphthyl benzoate. Chemical book 2-naphthyl benzoate, n.d. https://www.chemicalbook.com/SpectrumEN_93-44-7_IR1.htm (accessed 27, November, 2024).
[49] NIST chemical webbook, https://webbook.nist.gov/cgi/cbook.cgi?ID=C2005085&Mask=80#IR-Spec (accessed 27, November, 2024) n.d.